doi:10.1016/j.jmb.2010.06.056 J. Mol. Biol. (2010) 401, 776–791

JMB

Available online at www.sciencedirect.com

ScienceDirect

ELSEVIER

A Monomeric Photoconvertible Fluorescent Protein for Imaging of Dynamic Protein Localization

Hiofan Hoi[1], Nathan C. Shaner[2], Michael W. Davidson[3], Christopher W. Cairo[1,4], Jiwu Wang[2] and Robert E. Campbell[1]*

[1]*Department of Chemistry, University of Alberta, Edmonton, Alberta, Canada T6G 2G2*

[2]*Allele Biotechnology, 9924 Mesa Rim Road, San Diego, CA 92121, USA*

[3]*National High Magnetic Field Laboratory and Department of Biological Science, The Florida State University, 1800 East Paul Dirac Drive, Tallahassee, FL 32310, USA*

[4]*Alberta Ingenuity Center for Carbohydrate Science, Alberta, Canada*

Received 20 February 2010; received in revised form 15 June 2010; accepted 25 June 2010
Available online 13 July 2010

The use of green-to-red photoconvertible fluorescent proteins (FPs) enables researchers to highlight a subcellular population of a fusion protein of interest and to image its dynamics in live cells. In an effort to enrich the arsenal of photoconvertible FPs and to overcome the limitations imposed by the oligomeric structure of natural photoconvertible FPs, we designed and optimized a new monomeric photoconvertible FP. Using monomeric versions of *Clavularia* sp. cyan FP as template, we employed sequence-alignment-guided design to create a chromophore environment analogous to that shared by known photoconvertible FPs. The designed gene was synthesized and, when expressed in *Escherichia coli*, found to produce green fluorescent colonies that gradually switched to red after exposure to white light. We subjected this first-generation FP [named mClavGR1 (*m*onomeric *Clavularia*-derived *g*reen-to-*r*ed photoconvertible *1*)] to a combination of random and targeted mutageneses and screened libraries for efficient photoconversion using a custom-built system for illuminating a 10-cm Petri plate with 405-nm light. Following more than 15 rounds of library creation and screening, we settled on an optimized version, known as mClavGR2, that has eight mutations relative to mClavGR1. Key improvements of mClavGR2 relative to mClavGR1 include a 1.4-fold brighter red species, 1.8-fold higher photoconversion contrast, and dramatically improved chromophore maturation in *E. coli*. The monomeric status of mClavGR2 has been demonstrated by gel-filtration chromatography and the functional expression of a variety of mClavGR2 chimeras in mammalian cells. Furthermore, we have exploited mClavGR2 to determine the diffusion kinetics of the membrane protein intercellular adhesion molecule 1 both when the membrane is in contact with a T-lymphocyte expressing leukocyte-function-associated antigen 1 and when it is not. These experiments clearly establish that mClavGR2 is well suited for rapid photoconversion of protein subpopulations and subsequent tracking of dynamic changes in localization in living cells.

Keywords: fluorescent protein; photoconversion; protein engineering; fluorescence imaging

Edited by J. Karn

Introduction

In recent years, a handful of *Aequorea* green fluorescent protein (GFP) homologues cloned from anthozoan organisms have been reported to undergo irreversible photoconversion from a green fluorescent species to a red fluorescent species upon illumination with light of approximately 400 nm. To date, the naturally occurring photoconvertible proteins that have received the most attention are Kaede from coral *Trachyphyllia geoffroyi*,[1] EosFP from stony coral *Lobophyllia*

*Corresponding author. E-mail address: robert.e.campbell@ualberta.ca.

Present address: N. C. Shaner, Monterey Bay Aquarium Research Institute, 7700 Sandholdt Road, Moss Landing, CA 95039, USA.

Abbreviations used: FP, fluorescent protein; GFP, green fluorescent protein; StEP, staggered extension process; H2B, histone 2B; Cx43, connexin 43; ICAM-1, intercellular adhesion molecule 1; LFA-1, leukocyte-function-associated antigen 1; PBS, phosphate-buffered saline; DMEM, Dulbecco's modified Eagle's medium; FCS, fetal calf serum.

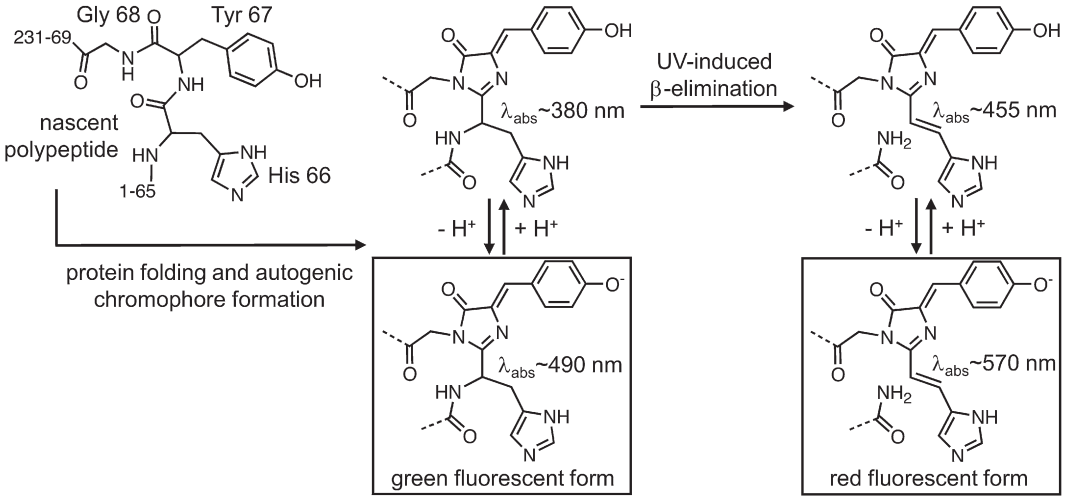

Fig. 1. Chromophore structure and UV-induced modifications of green-to-red photoconvertible FPs.[5] Residue numbers for the nascent polypeptide are for the mTFP1-derived variants described in this work. Broken lines represent connections to the polypeptide chain of the protein.

hemprichii,[2] and Dendra from octocoral *Dendronephthya* sp.[3] It has also been demonstrated that a naturally occurring nonphotoconvertible fluorescent protein (FP) can be engineered into a photoconvertible FP. Specifically, the photoconvertible FP known as KikGR was engineered from the green fluorescent variant KikG of the coral *Favia favus*.[4]

All green-to-red photoconvertible FPs characterized to date share a common His-Tyr-Gly-derived chromophore structure and a common photoconversion mechanism (Fig. 1).[5] The newly synthesized protein first folds into the characteristic β-barrel structure of the *Aequorea* GFP superfamily[6] and then undergoes the steps of posttranslational modification that lead to the formation of a green fluorescent chromophore with a conjugated system identical with that of *Aequorea* GFP chromophore. The chromophore can exist either in its neutral phenol form or in its anionic phenolate form (Fig. 1). Exactly where the equilibrium between these two forms lies is dependent on the local microenvironment of the chromophore (as determined by amino acid substitutions in close proximity to it) and the pH of the solution. The green-to-red photoconvertible FPs are distinguished from their nonphotoconvertible brethren by the respective consequences of exciting the neutral form, which absorbs most strongly at ~400 nm. In wild-type *Aequorea* GFP, the excited state of the neutral species undergoes excited-state proton transfer to form the anionic species, which then emits green fluorescence.[7] In the case of the green-to-red photoconvertible FPs, excitation of the neutral form leads to a break of the polypeptide chain through effective β-elimination of the residue immediately preceding the chromophore-forming His-Tyr-Gly tripeptide.[5,8] This elimination reaction results in the installation of a new double bond between C^{α} and C^{β} of the His residue, placing the side-chain imidazole in conjugation with the remainder of the avGFP-type chromophore. This extended conjugation decreases the energy gap between the highest occupied molecular orbital and the lowest unoccupied molecular orbital, and shifts the emission to the orange-to-red region of the visible spectrum. Photoconversion (i.e., a light-induced change in excitation or emission wavelength maxima) via alternate mechanisms has been observed in other color classes of FP.[9,10]

FP photoconversion allows researchers to 'highlight' a subpopulation of proteins within a cell or tissue through spatially defined illumination with a specific wavelength of light.[11] The subsequent dynamics of the highlighted protein can be followed due to its distinct fluorescence excitation and emission.[12,13] Optical highlighting can also be achieved using FPs that undergo so-called photoactivation (irreversible conversion from a nonfluorescent species to a fluorescent species upon illumination)[14] and photoswitching (reversible conversion between a nonfluorescent species and a fluorescent species upon illumination).[15] A more recent application of these types of proteins that has generated excitement in the cell biology community is superresolution fluorescence imaging.[16] This application also involves highlighting a subpopulation of protein molecules; however, instead of being in a spatially defined location, they are sparsely distributed throughout the whole sample to be imaged. The sample is then imaged to reveal the precise locations of the point sources of fluorescence, each of which corresponds to a single molecule of an FP. The sample is bleached, and the process is repeated. Many repetitions of this imaging protocol can produce images in which structures with dimensions of ~50 nm can be resolved.[17]

Kaede, the first example of an FP that can undergo irreversible green-to-red photoconversion upon illumination with UV light, was initially described by Ando *et al.* in 2002.[1] Unfortunately, the range of potential applications for Kaede remains limited by the fact that it is an obligate tetramer,[18] and no

monomeric variants have been reported. Unlike monomeric FPs, tetrameric FPs are generally detrimental to the proper trafficking and localization of recombinant fusion proteins.[19] In producing a monomeric green-to-red photoconvertible FP, the same workers appear to have had more success with engineered variants of the tetrameric KikGR FP, which is substantially brighter and more efficiently photoconverted than Kaede.[4] A monomeric version of KikGR, known as mKikGR, has recently been reported.[20]

The two other green-to-red photoconvertible FPs, EosFP and Dendra,[2,3] have been subjected to protein engineering to convert wild-type tetramers into monomers.[17,21] However, it is apparent that the monomeric version of EosFP retains a tendency to form dimers at higher concentrations.[17] The monomeric variant of EosFP, known as mEos, was created through the introduction of two point mutations that disrupted the protein–protein interfaces of the tetrameric species.[2,22] Expression of mEos at temperatures greater than 30 °C is problematic,[2] but an effectively monomeric tandem dimer variant does express well at 37 °C.[23] The poor expression of mEos at 37 °C has been overcome with the engineering of mEos2 through targeted substitution of residues with solvent-exposed side chains.[17] Although mEos2 has been reported to retain some propensity for dimer formation, this property does not appear to have adverse effects on the subcellular targeting of a variety of fusion proteins.[17]

The growing number of reports on optimized photoconvertible FPs reflects the growing demands on these proteins with respect to their enabling role in some popular cell biology applications. In particular, there is a continued need for bright and monomeric photoconvertible proteins, since these tools can enable the highest-precision superresolution fluorescence imaging.[17,20] In an effort to create a new monomeric photoconvertible FP with favorable properties, we embarked on a strategy distinct from that previously employed. Rather than start with a tetrameric photoconvertible protein and engineer it to be monomeric, we sought to start with a well-characterized monomeric coral-derived FP and engineer it to be a green-to-red photoconvertible FP. That tetrameric KikG was converted into KikGR through the use of protein design sets a precedent that it should be possible to convert a nonphotoconvertible FP into a photoconvertible FP.[4] Our starting template is a monomeric version of *Clavularia* sp. cyan FP (cFP484, a wild-type *Clavularia* cyan FP) known as mTFP1 (*m*onomeric *t*eal *FP 1*).[24]

Results and Discussion

Guided consensus design of a new photoconvertible FP

The new photoconvertible FP based on the mTFP1 template was designed using a strategy analogous to that previously used to design a consensus FP based on a monomeric Azami green template.[25] The known photoconvertible FPs, including EosFP,[1] Dendra2,[2] KikGR,[4] and Kaede,[3] were aligned to find the consensus at each amino acid position (Fig. 2). Amino acids of >50% consensus were maintained in the designed protein. At positions with no clear consensus, the corresponding residue in mTFP1 was used.[24] Residues of mTFP1 that had been substituted during the conversion of the wild-type cFP484 tetramer into a monomer were maintained in the design of the consensus protein. The designed gene was synthesized and, when expressed in *Escherichia coli*, found to exhibit green fluorescence that gradually switched to red after exposure to white light for 1–2 h. This variant was designated mClavGR1 (*m*onomeric *Clavularia*-derived *g*reen-to-*r*ed photoconvertible *1*) (Fig. 2). A complete list of all substitutions present in mClavGR1 and all other variants described in this work is provided in Supplementary Table 1.

Directed evolution with screening for photoconversion

Starting from mClavGR1, we undertook 11 rounds of evolution, where each round involved library creation by error-prone PCR[26] and staggered extension process (StEP) shuffling,[27] followed by a colony-based screen for those variants with the highest brightness and the highest ratio of red fluorescence after photoconversion to green fluorescence before photoconversion. In each round, approximately 6000 colonies were screened, and approximately 5–15 of the brightest variants were picked. A mixture of the plasmid DNA from these variants was then used as template for the subsequent round of library creation and screening. After the fourth round of evolution, we sequenced the clone with the highest fluorescence intensity in both the green channel (before photoconversion) and the red channel (after photoconversion). This clone, designated mClavGR1.1, was equivalent to mClavGR1 + T6bI, S34R, K36R, K74R, M113I, L166Q, Y173H (Fig. 2). A genealogy of all mClavGR variants is provided in Fig. 3a. Directed evolution starting from a template mixture of mClavGR1.1 and other bright variants was continued for seven more rounds. While we primarily relied on the diversity generated by error-prone PCR and StEP shuffling, we also created libraries in which specific positions that have previously been shown to improve the properties of homologous FPs were randomized (Fig. 3a; Supplementary Table 2). These rationally generated libraries were screened in a manner identical with that used for random libraries.

The brightest variant after the 11th round of directed evolution was equivalent to mClavGR1 + T6bI, T41I, D77E, F99Y, K115E, E127V, K139R, A183V (Fig. 3b). Characterization of the oligomeric state of this variant by gel-filtration chromatography revealed that the protein existed as a dimer (data not shown) and thus was designated dClavGR1.6,

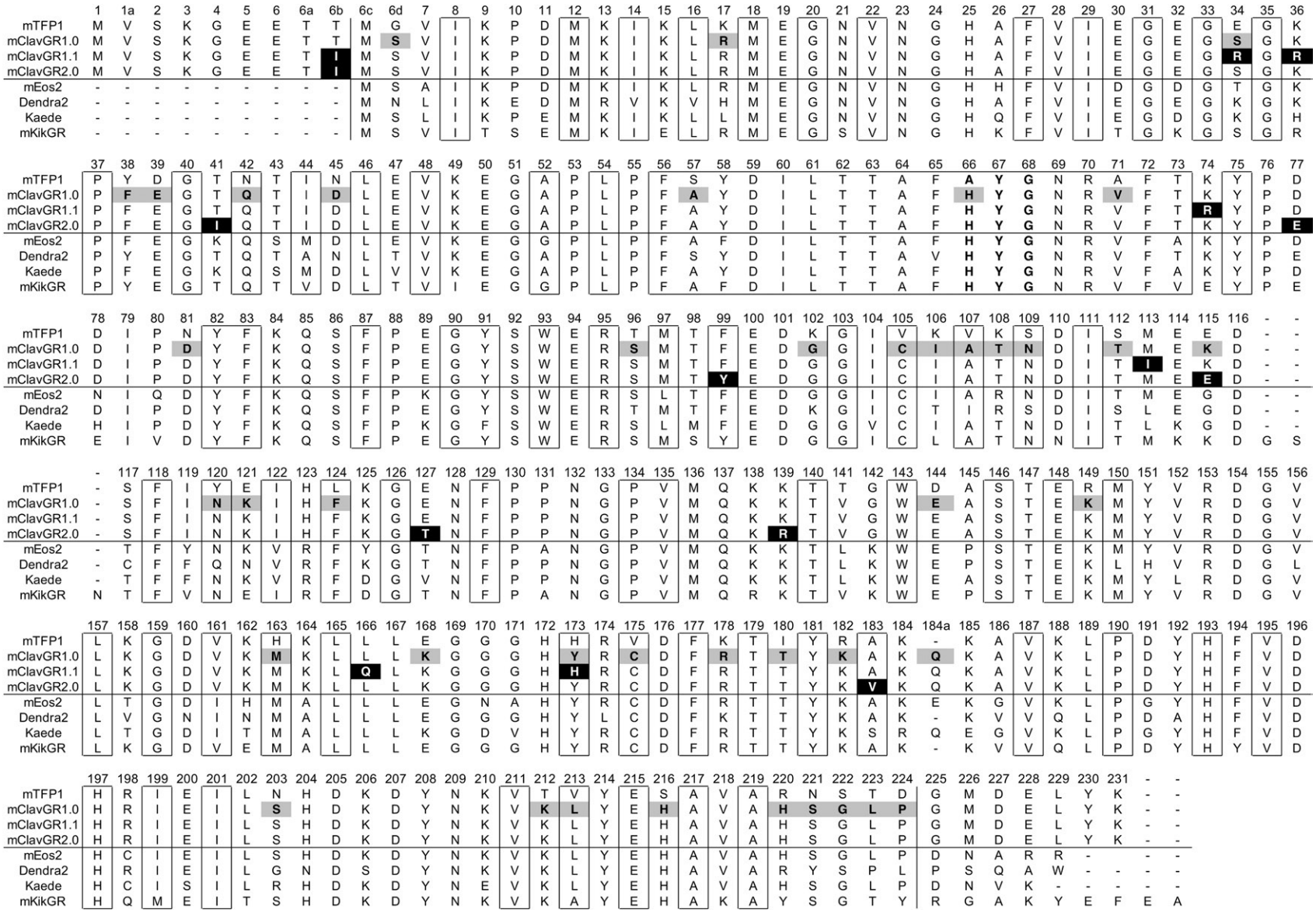

Fig. 2. Sequence alignment of mClavGR variants and other proteins relevant to this study. Substitutions in mClavGR1, relative to mTFP1, are represented as black text against a gray background. Substitutions in later mClavGR variants that were identified during the directed evolution are shown as white text against a black background. Residues with side chains directed towards the interior of the β-barrel are enclosed in black boxes. The chromophore-forming residues are numbered 66–68 in this alignment.

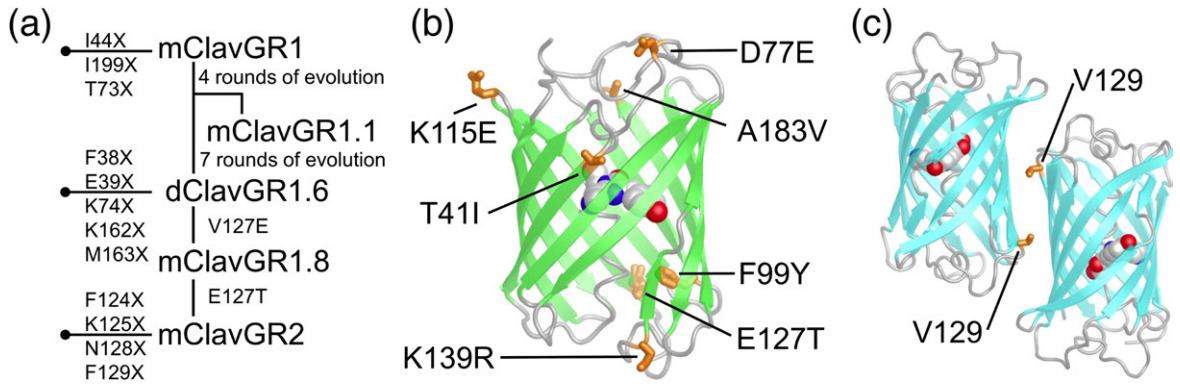

Fig. 3. Overview of the directed evolution of mClavGR. (a) A genealogy of ClavGR variants. The lines ending in filled circles indicate site-directed libraries that were created and screened but did not produce improved variants. An 'X' represents a selection of amino acids as specified in Supplementary Table 2. (b) Location of substitutions in mClavGR2 (relative to mClavGR1) that were introduced during the directed evolution process. The X-ray crystal structure of mTFP1 (Protein Data Bank ID 2HQK) is used here to represent mClavGR.[24] (c) The dimer of amFP486 (Protein Data Bank ID 2A48) showing the location of valine 129, which is structurally homologous to residue 127 of mClavGR.[24,28] As discussed in the text, substitutions at this position can influence the oligomeric state of the protein.

where the prefix 'd' indicates a dimer. dClavGR1.6 is about 5-fold brighter than mClavGR1 when expressed in *E. coli* and shares only the T6bI substitution with mClavGR1.1. Analysis of the substitutions present in dClavGR1.6, in combination with a structure-based alignment of the X-ray structures of mTFP1 and tetrameric amFP486,[24,28] led us to suspect that the E127V substitution was most likely responsible for reconstituting the dimer interface (Fig. 3c). Accordingly, we introduced the single amino acid reversion V127E into dClavGR1.6 by site-directed mutagenesis to produce mClavGR1.8. Although mClavGR1.8 was monomeric, it retained only 50% of the fluorescent brightness of dClavGR1.6 when expressed in *E. coli*. Noting that the V123T substitution had been previously used to convert EosFP into mEos,[17] and that position 123 of EosFP aligns with position 127 of mClavGR1.8, we introduce the E127T substitution into mClavGR1.8. The resulting protein, designated mClavGR2 (Figs. 2 and 3b), had regained 60% of the brightness of dClavGR1.6 when expressed in *E. coli* and retained the monomeric character of mClavGR1.8 as determined by gel-filtration chromatography at a concentration of 1 mM (Supplementary Fig. 1). Under the same experimental conditions, Dendra2 was also monomeric, but mEos2 existed as a dimer or higher-order oligomer at concentrations of 0.1 mM and greater. Further efforts to improve the protein by screening libraries in which residues of interest were randomized (Fig. 3a; Supplementary Table 2) did not result in identification of further improved variants.

In vitro characterization of mClavGR2

As described in Directed Evolution with Screening for Photoconversion, we used an empirical screening process in order to produce a protein that had an optimal combination of brightness and photoconversion efficiency. In order to determine what changes in the spectral properties of the protein

Table 1. Properties of mClavGR variants and other monomeric photoconvertible FPs discussed in this work

Protein		λ_{ab} (nm)	λ_{em} (nm)	ε (mM^{-1} cm^{-1})	Φ	Brightness (mM^{-1} cm^{-1})[a]	pK_a	Photostability (s)[b] Wide field	Photostability (s)[b] Confocal	$\Phi_{PC,GRX}/\Phi_{PC,GR1}$[c]	$E_{PC,GRX}/E_{PC,GR1}$[d]
mClavGR1	Green	486	503	16	0.84	14	8.0	14	202	1.0	1.0
	Red	565	582	21	0.56	12	7.4	64	5002		
mClavGR2	Green	488	504	19	0.77	15	8.0	17	233	1.2	1.8
	Red	566	583	32	0.53	17	7.3	175	3644		
mEos2[e]	Green	506	519	56	0.84	47	5.6	42	240		
	Red	573	584	46	0.66	30	6.4	323	2700		
Dendra2[e]	Green	490	507	45	0.50	23	6.6	45	260		
	Red	553	573	35	0.55	19	6.9	378	2420		
mKikGR[e]	Green	505	515	49	0.69	34	6.6	14	80		
	Red	580	591	28	0.63	18	5.2	21	530		

[a] Product of ε and Φ. For comparison, the brightness of mCherry is 16 mM^{-1} cm^{-1}, and the brightness of EGFP is 34 mM^{-1} cm^{-1}.[29]
[b] Time to photobleach from 1000 photons s^{-1} $molecule^{-1}$ to 500 photons s^{-1} $molecule^{-1}$ under wide-field and confocal illumination, respectively.
[c] Photoconversion quantum yield (calculated using Eq. (1)) relative to mClavGR1.
[d] Photoconversion contrast (calculated using Eq. (2)) relative to mClavGR1.
[e] Previously reported values.[17,20,30]

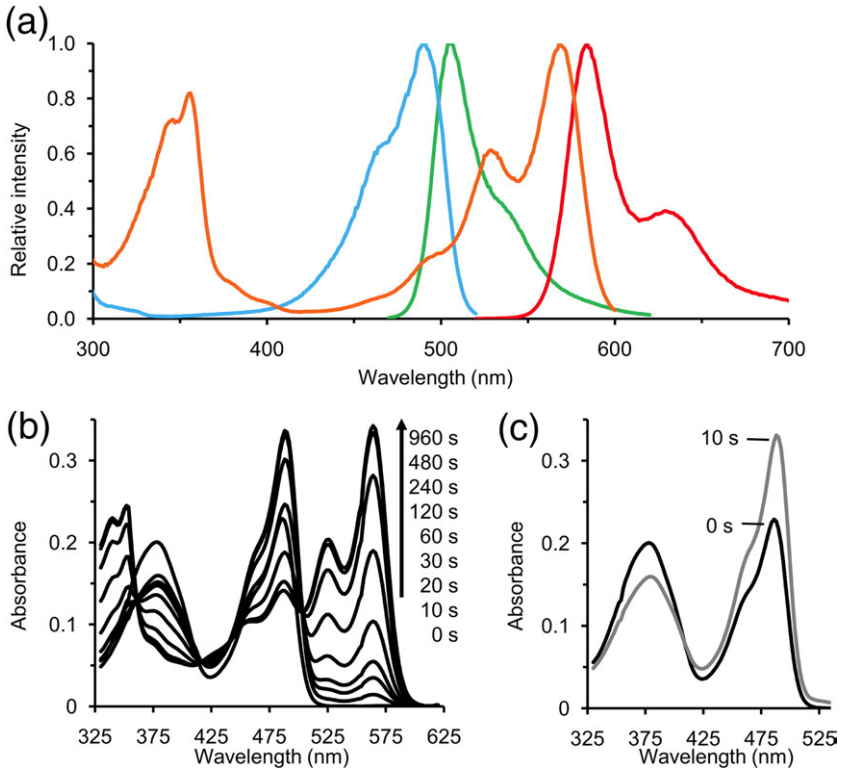

Fig. 4. Spectral changes in mClavGR2 upon photoconversion. (a) Excitation (cyan and orange) and emission (green and red) fluorescence spectra of the green state (before photoconversion) and the red state (after photoconversion) of mClavGR2, respectively. (b) Absorbance spectra *versus* photoconversion time of mClavGR2 in PBS (pH 7.4). The light source used for photoconversion is the 405-nm light-emitting-diode-based illumination chamber used for photoconverting the protein in bacterial colonies. (c) Brief illumination (10 s) with 405-nm light causes a substantial increase in the absorbance of the green fluorescent species.

had resulted in the observed improvements in its properties, we undertook a thorough *in vitro* characterization of mClavGR1 and mClavGR2 (Table 1). An overall conclusion from the *in vitro* characterization experiments is that mClavGR2 has spectral properties that are comparable to those of the other members of the class of green-to-red photoconvertible FPs.[17] This result is consistent with the fact that all of the known green-to-red photoconvertible FPs, including mClavGR2, have high sequence homologies, particularly when one considers only those residues with side chains directed towards the interior of the β-barrel (discussed below).

Prior to illumination, purified mClavGR2 protein has an excitation maximum at 488 nm and an emission maximum at 504 nm (Fig. 4a). Illumination with the same 405-nm light source used to photoconvert colonies of *E. coli* causes the formation of a new species with primary excitation maximum at 566 nm and emission maximum at 583 nm. As represented in Fig. 1, it is the anionic form of the chromophore that is the primary fluorescent species in both the green fluorescent state and the red fluorescent state. Interestingly, the red fluorescent state has a second strong excitation peak at 355 nm. This situation is reminiscent of the excitation spectrum of *Aequorea* GFP, which also exhibits two peaks. In *Aequorea* GFP, the higher-energy excitation peak is caused by the protonated form absorbing a photon, undergoing excited-state proton transfer, and then fluorescing from the anionic excited state.[7] An analogous explanation does not satisfactorily explain the mClavGR2 excitation spectrum, since the protonated form of the mClavGR2 red-state chromophore absorbs at 455 nm, 100 nm redshifted from the 355-nm excitation peak (Supplementary Fig. 2c). Adam *et al.* rationalized a similarly positioned peak observed in the excitation spectrum of Dendra2 as being due to a higher-energy electronic transition of the red state of the chromophore.[21]

Prior to illumination, the absorbance spectrum of mClavGR2 is dominated by two distinct peaks (Fig. 4b): one at 380 nm, which is attributable to the neutral phenol form of the chromophore, and the other at 488 nm, which is attributable to the anionic phenolate form of the chromophore (refer to Fig. 1). Of these two peaks, only the phenolate form also appears in the excitation spectrum (Fig. 4a), indicating that only this form is green fluorescent. The neutral phenol form is not green fluorescent but, as previously established by the action spectra of Kaede,[1] EosFP,[2] and Dendra2,[21] is the form that can undergo photoconversion into the red state when excited (refer to Fig. 1). Indeed, recording of absorbance spectra at regular intervals during otherwise continuous illumination with the 405-nm light source revealed a monotonic increase in the 566-nm absorbance peak and a monotonic decrease in the 380-nm peak (Fig. 4b). The absorbance of the 488-nm peak also undergoes an eventual decrease with continued illumination, illustrating that the phenol and phenolate forms of the green state of mClavGR2 are in equilibrium and subject to the law of mass action.

An interesting property of mClavGR2 is that the 405-nm illumination used to photoconvert the neutral phenol form of the green state can also

temporarily drive the phenol/phenolate equilibrium of the green state towards the anionic form. Specifically, we observed that both the absorbance at 488 nm (Fig. 4c) and the overall fluorescence of the phenolate form increase immediately after illumination with 405-nm light. In the subsequent absence of the 405-nm light, the absorbance at 488 nm (and fluorescence at 504 nm) decreases to its original level over several tens of seconds. A similar phenomenon has also been reported to occur with Kaede[31] and Dendra2.[10] We speculate that this shift in equilibrium could be the result of photoinduced cis–trans isomerization of the chromophore similar to that observed to occur for the green state of the variant of EosFP known as IrisFP.[32] An alternative explanation is that illumination shifts the phenol/phenolate equilibrium towards the phenolate state. However, if this were the case, we would expect equilibrium to be reestablished on a timescale of milliseconds as determined for analogous proton transfer processes in *Aequorea* GFP[33] and Kaede,[31] not on the tens of seconds that we observe in mClavGR2. We have not observed any reversible photoswitching or photoconversion of the red state of the chromophore.

Although both the green state and the red state of mClavGR2 are approximately five times brighter than those of mClavGR1 when expressed in *E. coli*, its inherent brightness (i.e., the product of ε and Φ) has improved only by a modest 7% and 42% for the green and red states, respectively (Table 1). This indicates that the improvement of brightness seen in *E. coli* is very likely due to a more complete maturation or a more efficient folding of the FP. mClavGR2 further benefits from a 20% increase in the quantum yield of photoconversion (Φ_{PC}) relative to mClavGR1. The combination of the improved inherent brightness of the red state and the improved Φ_{PC} provides an overall 80% improvement in photoconversion contrast (E_{PC}). E_{PC} is a relative measure of the overall intensity of red fluorescence that can be generated from a fixed concentration of protein molecules.

Structure-based comparison of mClavGR2 and other green-to-red photoconvertible FPs

Of the previously reported green-to-red photoconvertible FPs, mClavGR2 has the highest amino acid percentage identity with mEos2 (Fig. 2; Supplementary Tables 3 and 4).[17] However, if one considers only those residues with side chains directed towards the interior of the β-barrel, mClavGR2 is most similar to mKikGR, with a relatively conservative amino acid difference of only 7 (*versus* 8 for Kaede, 9 for mEos2, and 13 for Dendra2) (Supplementary Tables 5 and 6). Of the green-to-red FPs reported to date, the two that are most similar with respect to the identity of residues directed towards the interior of the β-barrel are mEos2 and Kaede, with a difference of only 4. The two that are most divergent are Dendra2 and mKikGR, with a difference of 17. As mentioned above, the similar photophysical characteristics of the members of this class of FPs are attributed to the fact that they are all very similar with respect to their interior residues and chromophore environments.

One of the most distinctive amino acid differences in close proximity to the chromophore is the residue at position 73. In mClavGR2 and Dendra2 (numbered as residue 69), this residue is Thr; in mEos2 and Kaede, it is Ala; and in mKikGR, it is Val (Fig. 2; Supplementary Table 5). It has previously been suggested that hydrogen bonding between the side chain of Thr at this position and the guanidinium group of Arg70 (Arg66 in Dendra2) may hold the guanidinium farther from the chromophore and thus limit charge stabilization.[21] This diminished degree of charge stabilization in Dendra2 has been used to explain both the blueshifted emission and the higher apparent pK_a of the chromophore.[21] We attempted to improve the properties of mClavGR1 by introducing substitutions at position 73. When we generated a library of all possible substitutions at position 73 and screened it in colonies to identify the variants that exhibited the highest green fluorescence before photoconversion and the highest red fluorescence after photoconversion, we found that the brightest colonies retained Thr at position 73. We also created the Thr73Ala and Thr73Val variants individually and characterized them. When expressed in *E. coli*, the green state of the Thr73Ala variant was approximately equivalent in brightness to the Thr73 progenitor, but the red (photoconverted) state was substantially dimmer. For the Thr73Val variant, both the green state and the red state were substantially dimmer than the original Thr73 variant.

There are only two residues of mClavGR2 that are directed towards the interior of the β-barrel and have amino acid identities that are not found in any of the other green-to-red photoconvertible FPs (Supplementary Table 5). These residues are Ile44 (Met, Ala, and Val in others) and Val183 (Ala and Ser in others). The valine at position 183 is the result of an amino acid substitution (Ala183Val) identified through screening of randomly mutated libraries for improved brightness and photoconversion. This is located near one end of the ninth β-strand of the protein and is relatively distant from the chromophore. Given its distant location, it is unlikely that Val183 has a direct influence on the properties of the chromophore and more likely contributes to improved brightness by increasing the folding efficiency of the protein. In contrast, Ile44 is in very close proximity to the chromophore and likely interacts with the side chain of His66, which is an integral part of the red chromophore. We generated a saturation library at Ile44 and again found that the best-performing variant remained to be Ile. We also created the Ile44Met and Ile44Val variants individually. We found that the Met substitution produced a variant with diminished photoconversion efficiency and that the Val substitution produced a variant with dimmer fluorescence in both the green state and the red state.

Phenol/phenolate equilibrium and photoconversion

The pH-dependent absorption spectra of the green and red states of mClavGR2 are shown in Supplementary Fig. 2. With apparent pK_a values of 8.0 and 7.3, respectively, both states of the chromophore exhibit substantial pH sensitivity in the physiological pH range (Table 1). It is notable that mClavGR2 has the highest pK_a reported for any of the green-to-red photoconvertible FPs.[17] Due to our extensive empirical optimization, we expect the pK_a value for the green species to be near an optimal value with respect to photoconversion efficiency. That is, with this pK_a value, a substantial portion of the protein exists in the neutral phenol form at pH 7.4 and, thus, the overall rate of photoconversion is increased. A similar relationship between higher pK_a and enhanced photoconversion efficiency has been noted for both KikGR and Dendra2. In the case of KikGR, directed evolution for brighter red fluorescence following photoconversion resulted in a shift of the green-state pK_a from an initial value of 4.2 to a final value of 7.8.[4] This change dramatically shifted the phenol/phenolate equilibrium towards the neutral form at pH 7.4. In the case of Dendra2 (pK_a = 7.1), it was noted that the 20-fold improvement in photoconversion efficiency relative to EosFP (pK_a = 5.8) is fully explained by the 20-fold higher concentration of the phenol form under physiological conditions.[21] Presumably, the phenol/phenolate equilibrium in mClavGR2 could be shifted even further to the neutral form in variants with an even higher pK_a. In this case, the intensity of the green fluorescence would have been further diminished. Accordingly, the optimal pK_a of the green state represents a compromise between the desirable but conflicting demands of high photoconversion efficiency and high brightness of the green state.

While the pK_a of the green state of mClavGR2 may be close to optimal, it would be preferable to have a lower pK_a for the red state of mClavGR2. A lower pK_a is beneficial for two reasons: first, there are fewer potential artifacts due to local changes in pH; and, second, the protein is brighter due to a greater fraction of the protein existing in the red fluorescent phenolate form, as opposed to the nonfluorescent phenol form. In mTFP1 (pK_a = 4.3), the imidazole side chain of His163 is hydrogen bonded to the phenolate moiety of the chromophore.[24,34] In mClavGR2, this residue has been substituted with a Met, which should be much less effective at stabilizing the anionic form and almost certainly contributes to the dramatically increased pK_a. In an effort to decrease the pK_a of the red state of mClavGR2, we generated the mClavGR2 Met163His variant, even though it seemed likely that this substitution would decrease the pK_a of both the green state and the red state. Not unexpectedly, the green state of this variant was found to exist entirely in the anionic phenolate form at physiological pH, and photoconversion thus proceeded with very poor efficiency.

Live cell imaging of various mClavGR2 fusion proteins

Given the results of our characterization experiments, it is apparent that there are some potential advantages and some potential disadvantages of mClavGR2 relative to other members of the class of green-to-red photoconvertible FPs with respect to applications in the imaging of dynamic protein localization. Most notable among the advantages of mClavGR2 are its monomeric structure, its highly optimized and relatively rapid folding efficiency (Supplementary Fig. 3), and its high photoconversion efficiency due to the high pK_a of the green state. The primary disadvantage is the high pK_a of the red state (Table 1; Supplementary Fig. 2), which causes the protein to have approximately half of its maximal fluorescent brightness under physiological pH conditions. It should be noted that the red state of mClavGR2, despite having only approximately half of its maximal brightness, retains brightness slightly greater than the red state of the popular red FP known as mCherry at pH 7.4 (Table 1).[35]

Another advantage of mClavGR2 that became apparent while we were performing photobleaching experiments with protein expressed in live cells is the improved photostability of the red state of the protein under confocal illumination conditions relative to other green-to-red photoconvertible FPs. The time to bleach the red state to 50% of the initial intensity for mClavGR2 (3644 s; see Table 1 and Supplementary Fig. 4) represents a substantial improvement over mEos2 (2700 s) and Dendra2 (2420 s).[17] Oddly, this advantage does not extend to wide-field illumination conditions where the time to bleach to 50% of the initial intensity for mClavGR2 (175 s) is somewhat lower than those reported for mEos2 (323 s) and Dendra2 (378 s). It should be noted that the red state of mKikGR exhibits relatively rapid photobleaching under both wide-field (21 s) and confocal (530 s) illumination conditions. The time to bleach the green state of mClavGR2 to 50% of its initial intensity using confocal illumination (233 s) is only slightly faster than those of both mEos2 (240 s) and Dendra2 (260 s), but substantially slower than that of mKikGR (80 s). For wide-field photobleaching, mClavGR2 (17 s) is more similar to mKikGR (14 s) than it is to the more photostable mEos2 (42 s) and Dendra2 (45 s) variants.

In an effort to determine if mClavGR2 is potentially useful for the imaging of dynamic protein localization, we have assembled mammalian expression plasmids for a variety of mClavGR2 constructs, used these plasmids to transfect cultured mammalian cells, and acquired fluorescence images of the resulting cells both before photoconversion and after photoconversion. Following expression of mClavGR2 in HeLa cells as an unfused protein, we were able to photoconvert the protein in a localized region and to image the subsequent diffusion of the red-state protein as it evenly dispersed throughout the cytoplasm over a timescale of approximately 30 s

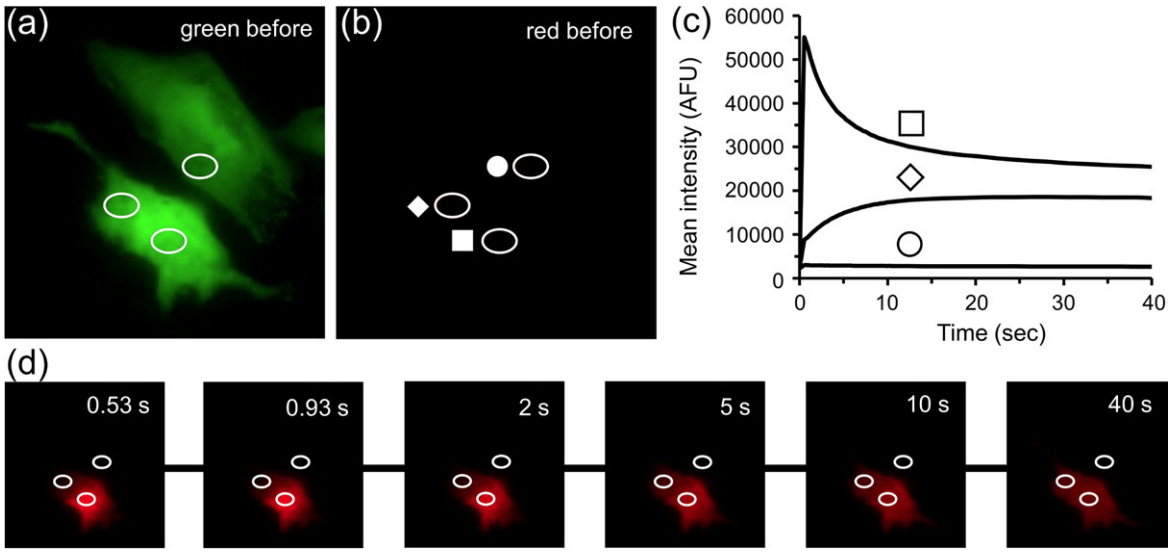

Fig. 5. Photoconversion of unfused mClavGR2 in live cells. (a) Green fluorescence image from two cells expressing mClavGR2 prior to photoconversion. (b) The same cells as in (a) imaged using a filter set for red fluorescence prior to photoconversion. The three areas of interest are indicated with a circle, diamond, and square. The area indicated with a square corresponds to the location where the cell is illuminated with a 408-nm laser from $t = -2$ to 0 s. (c) Mean red fluorescence intensities in each of the areas of interest marked in (b). (d) A series of images showing the free diffusion of photoconverted mClavGR2. Indicated times represent time elapsed since the end of the 408-nm laser illumination.

(Fig. 5). This experiment established that mClavGR2 did not exhibit any anomalous localization when expressed alone in cells and was capable of free and rapid diffusion in the cytoplasm.

Encouraged by these promising results, we proceeded to construct fusion constructs in order to test whether mClavGR2 could be fused to different protein partners and targeting sequences without causing mistargeting or possible misfolding of either protein. In Fig. 6, we show images of the green state of mClavGR2 in 16 commonly used fusion constructs. These localization patterns for all fusion constructs were judged to be indistinguishable from the localization patterns of the analogous *Aequorea* GFP constructs imaged under identical conditions in the same laboratory. The favorable performance of mClavGR2 in these constructs serves as ancillary evidence of its monomeric state. Notably, the fine filament structure of the actin cytoskeleton is clearly preserved with the mClavGR2-β-actin fusion expressed in HeLa cells (Fig. 6a). For histone 2B (H2B), connexin 43 (Cx43), and Rab5a fusion constructs, we performed localized photoconversion and subsequent imaging of the dynamic localization of both green fluorescence and red fluorescence. Two-color image sequences for these experiments are provided as Supplementary Figs. 5–7, and time-lapse movies are available online as Supplementary Movies 1–3. These experiments established that mClavGR2, when fused to other proteins, causes minimal perturbation of localization and trafficking dynamics. Furthermore, the green and red states of mClavGR2 have sufficient brightness and photostability for long-term imaging experiments.

To further test the utility of mClavGR2 and to fully exploit the advantages provided by its monomeric structure, we investigated whether mClavGR2 could be used to monitor the dynamics of a transmembrane adhesion protein, intercellular adhesion molecule 1 (ICAM-1). We specifically asked whether we could quantitatively assess changes in the lateral mobility of ICAM-1 on the surface of a mammalian cell while engaged in cell–cell contact with a T-lymphocyte (Jurkat) cell expressing the ICAM-1 receptor leukocyte-function-associated antigen 1 (LFA-1). ICAM-1 lateral mobility has been shown to be mediated by cortactin, filamin B, and adhesion receptor microdomains.[36–38] Fluorescent images of HeLa cells transiently transfected with a plasmid encoding ICAM-1-mClavGR2 revealed an unambiguous pattern of surface FP localization (Fig. 7a) consistent with the expected localization of ICAM-1 in the plasma membrane. Incubation of these adherent cells with a suspension of Jurkat cells resulted in the formation of cell–cell contacts where a Jurkat cell had settled onto the plasma membrane of a HeLa cell. Bright-field imaging was used to identify Jurkat cells in apparent physical contact with transfected HeLa cells (Fig. 7b). For each apparent contact, the existence of specific ICAM-1/LFA-1-mediated contact was confirmed by locating a bright cluster of fluorescence at the contact point suggested by the bright-field images (Fig. 7c and d). Localized photoconversion at the point of contact was performed, and a time series of red fluorescence images was acquired to trace the diffusion of ICAM-1 initially found at the contact zone (Fig. 7e). Identical experiments were performed at arbitrary locations on the plasma membrane of transfected HeLa cells in the absence of Jurkat cells. Postcollection analysis was used to extract the fluorescence intensity at the contact point as a function of time (Fig. 8a).

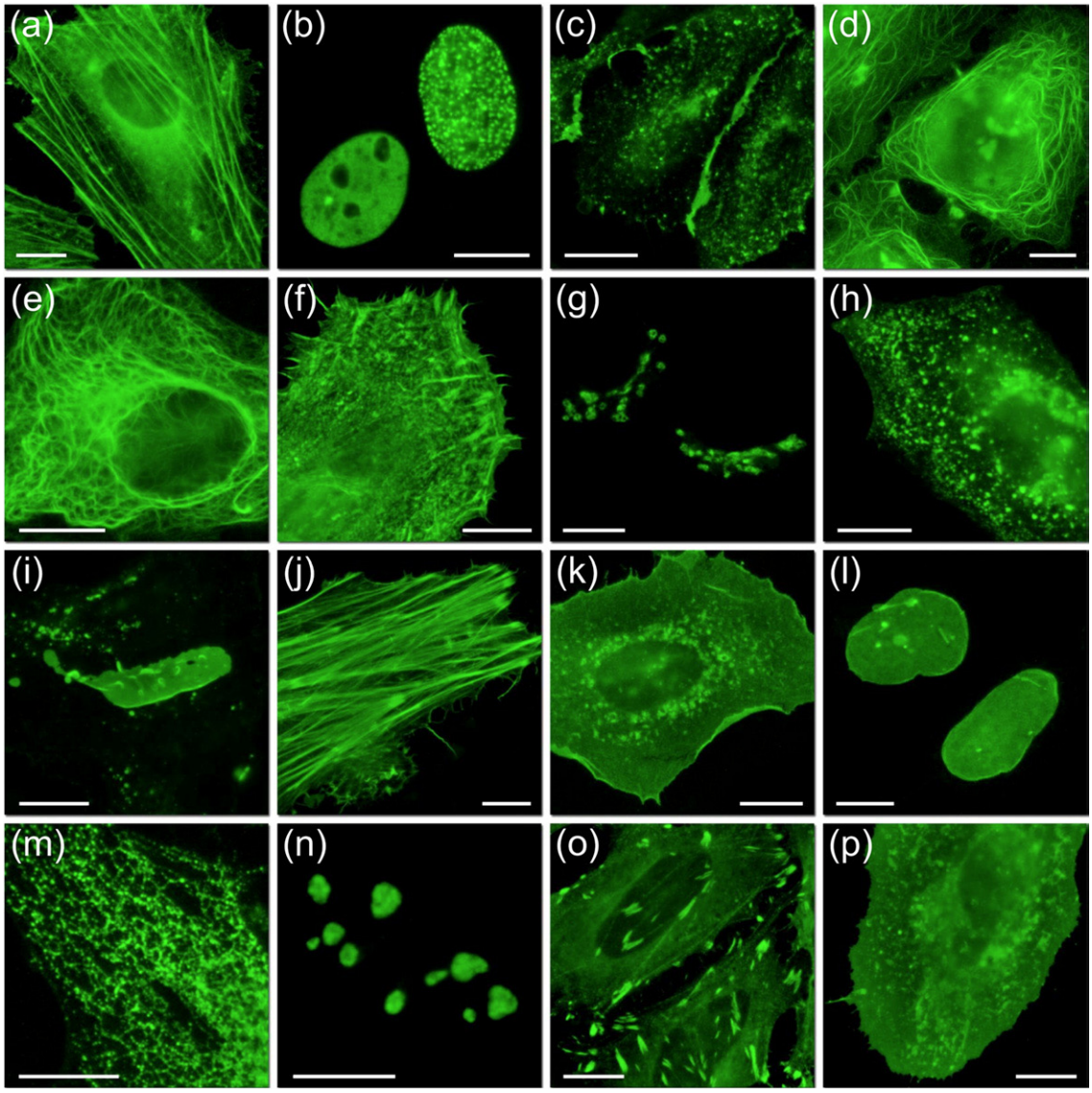

Fig. 6. Live cell imaging of mClavGR2 protein fusions. The fusion peptide or protein is listed as C-terminal or N-terminal to mClavGR2, followed by the number of amino acids in the linker separating the two domains: (a) mClavGR2-actin-C-7; (b) mClavGR2-CAF1-C-10 (human chromatin assembly factor 1); (c) mClavGR2-VE-cadherin-N-10; (d) mClavGR2-MAP4-C-10 (microtubule binding domain of mouse MAP4); (e) mClavGR2-keratin-N-17 (human cytokeratin 18); (f) mClavGR2-α-actinin-N-19; (g) mClavGR2-GAL-T-N-7 (Golgi complex); (h) mClavGR2-Rab5a-C-7; (i) mClavGR2-Cx43-N-7; (j) mClavGR2-lifeact-N-7 (yeast actin binding protein); (k) mClavGR2-c-src-N-7 (chicken c-src); (l) mClavGR2-lamin B1-C-10; (m) mClavGR2-ER-N-5 (calreticulin signal sequence N-terminal and KDEL C-terminal); (n) mClavGR2-fibrillarin-C-7; (o) mClavGR2-zyxin-N-6; (p) mClavGR2-c-Ha-Ras (CAAX)-C-5 (farnesylated membrane targeting signal). All fusions were expressed in HeLa cells (CCL-2; ATCC) for imaging.

Our analysis of ICAM-1 diffusion revealed that the diffusion half times increased from 6.6±0.4 s for proteins not involved in cell–cell contacts to 22.9±3.7 s for proteins involved in cell–cell contacts (Fig. 8b). This result suggests an almost 4-fold reduction in the rate of diffusion of ICAM-1 found within a contact zone *versus* ICAM-1 found elsewhere on the cell surface. Regardless of whether or not ICAM-1 was in adhesive contact, approximately 25% (24±4% or 26±2%, respectively) of the protein was effectively immobile over the 100-s timescale of the experiment (Fig. 8b). These results are consistent with previous reports indicating that ICAM-1 mobility is reduced by cross-linking of the receptor, although cross-linking here is induced by the presentation of receptors as part of the lymphocyte cell surface.[36] These results unambiguously demonstrate that photoconversion of mClavGR2-containing constructs will be a powerful tool for dissecting the mechanisms that mediate cellular adhesion by allowing long-term tracing of receptors and lateral diffusion measurements.

Summary

We have developed and characterized a new green-to-red photoconvertible FP variant known as

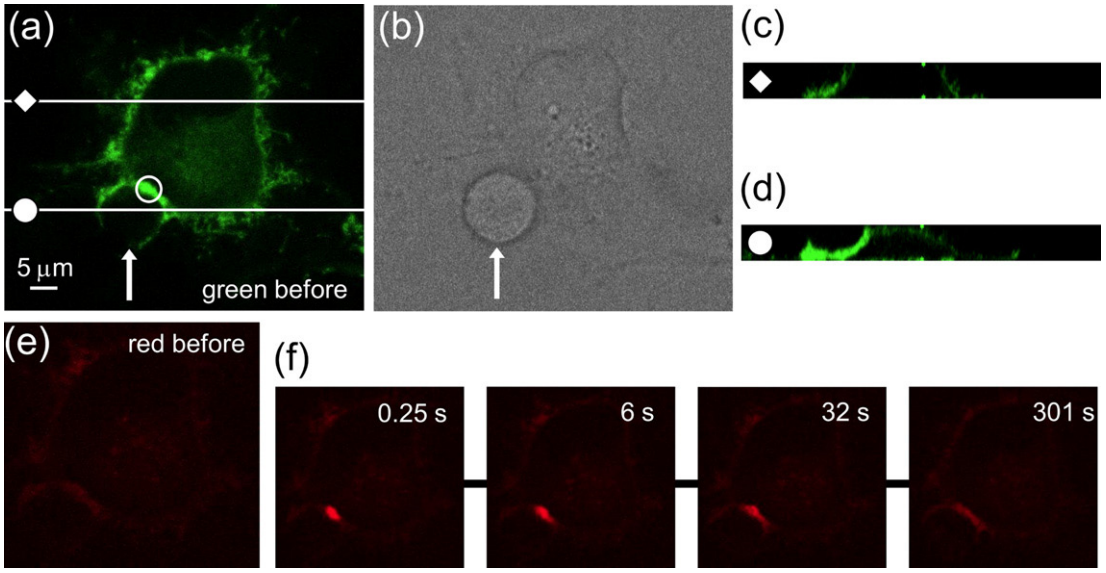

Fig. 7. Photoconversion of ICAM-1-mClavGR2 on a HeLa cell in contact with a Jurkat cell expressing LFA-1. (a) Green fluorescence image of a HeLa cell in contact with a Jurkat cell. The arrow indicates the location of the Jurkat cell as shown in (b). Brighter fluorescence is observed at the cell–cell contact point due to the interaction of LFA-1 on the surface of the Jurkat cell with ICAM-1-mClavGR2 on the HeLa cell. The white circle at the cell–cell contact is the area to be photoconverted. Diagonal lines marked with a diamond and a circle correspond to the reconstructed x–z cross sections represented in (c) and (d). (b) Bright-field image of the same field of view as (a) with focus adjusted to show the Jurkat cell (white arrow). (c) Cross-sectional view of cells shown in (a) at the line indicated with a diamond. (d) Cross-sectional view of the cell shown in (a) at the line indicated with a circle. (e) Red fluorescence image of the same field of view as (a) prior to photoconversion. (f) Time-lapse images of the red fluorescence following photoconversion.

mClavGR2. Unlike other members of this class of FP, mClavGR2 was engineered from a well-characterized and monomeric FP progenitor. Our results demonstrate that mClavGR2 has favorable spectral properties, retains the monomeric structure of its progenitor, and, in the constructs tested to date, does not interfere with the correct localization of a genetically fused protein partner. We anticipate this new addition to the toolbox of engineered FPs to be of great utility in imaging fast protein dynamics in live cells. Experiments aiming to determine whether the advantages of mClavGR2 translate into improved performance in superresolution imaging applications have been initiated.[16]

Materials and Methods

General methods and materials

All synthetic DNA oligonucleotides for cloning and library construction were purchased from Integrated DNA Technologies (Coralville, IA). PCR products and products of restriction digests were purified using the QIA

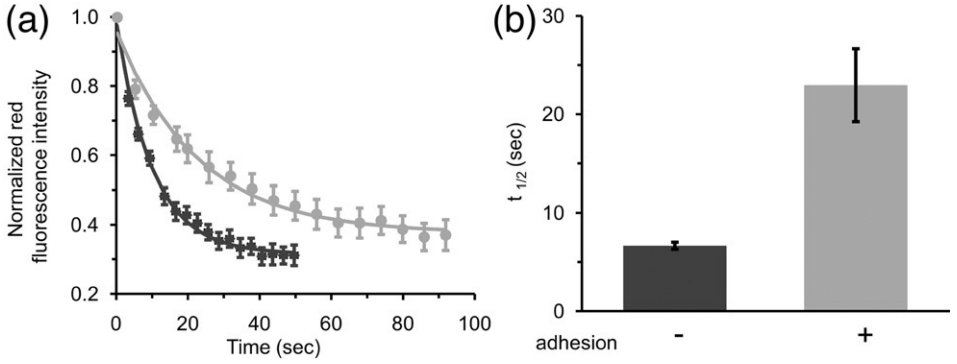

Fig. 8. Diffusion of ICAM-1-mClavGR2 on the plasma membrane. (a) Red fluorescence intensity at the location of photoconversion *versus* time after photoconversion for HeLa cells either at the point of adhesion with Jurkat cells (circles) or at an arbitrary point on the plasma membrane in the absence of Jurkat cells (squares). Data represent the average results from 8 and 22 independent measurements, respectively. Lines represent the best fit of the data using Eq. (3). (b) Summary of diffusion times ($t_{1/2}$) as obtained by fitting of the data provided in (a). The $t_{1/2}$ values for the two data sets are significantly different ($p<0.01$). The 'adhesion' label refers to whether or not the site of photoconversion was within an adhesion contact, as identified in bright-field and fluorescence images.

gel extraction kit (Qiagen) in accordance with the manufacturer's protocols. Restriction enzymes were purchased from New England Biolabs. The cDNA sequences for all mClavGR variants were confirmed by dye terminator cycle sequencing using the DYEnamic ET kit (Amersham Biosciences) or the BigDye Terminator v3.1 Cycle Sequencing Kit (Applied Biosystems). Sequencing reactions were analyzed at the University of Alberta Molecular Biology Service Unit or the Florida State University Department of Biological Science DNA Sequencing Facility.

Plasmid library creation and site-directed mutagenesis

For production of the designed cDNA encoding mClavGR1, 14 forward oligonucleotides and 14 reverse oligonucleotides with 51 bases each were synthesized and assembled using circular assembly amplification.[39] A forward primer with an XhoI restriction site and a reverse primer with an EcoRI restriction site were used to amplify the cDNA, which was subsequently digested and ligated into a similarly digested pBAD/His B vector (Invitrogen). Randomly mutated libraries were created by error-prone PCR, where dNTPs mixed with a deficient component were used, and $MnCl_2$ was added to the reaction to further decrease the fidelity of *Taq* polymerase.[26] Saturation/semisaturation mutagenesis at specific residues was performed using overextension PCR, as previously described.[24] StEP PCR was performed as previously described.[27] Specifically, 0.1 pmol of pBAD/His B plasmids containing a DNA sequence of 5–15 mClavGR variants selected from randomly mutated libraries was used as template mix. The mixture was subjected to 100 cycles (94 °C for 45 s, then 55 °C for 5 s), followed by an extra extension step at 72 °C for 5 min. Regardless of library assembly method (i.e., error-prone PCR, saturation mutagenesis, or StEP PCR), gene libraries were inserted into pBAD/His B between the XhoI site and the EcoRI site, as described above. Electrocompetent *E. coli* strain DH10B (Invitrogen) was transformed and plated on LB agar plates supplemented with ampicillin (0.1 mg/ml) and L-arabinose (0.2%). Plates were incubated for 14 h at 37 °C prior to screening.

Plasmid library screening

E. coli colonies expressing the mClavGR libraries were grown on 10-cm Petri dishes. In order to screen libraries for variants that were brighter and exhibited more efficient photoconversion, we developed a method for photoconverting FPs expressed in colonies of *E. coli*. Our method involves a three-step process. In the first step, a custom imaging system equipped with filter sets (Chroma) for 470/40 nm excitation with 510/20 nm emission (i.e., for green fluorescence) and filter sets for 560/40 nm excitation with 630/60 nm emission (i.e., for red fluorescence) is used to acquire both green and red fluorescence images of the Petri dish. In the second step, the dish is placed in a 'photoconversion chamber,' where it is evenly illuminated with light from six 9×11 arrays of 405-nm light-emitting diodes (OptoDiode Corporation, Newbury Park, CA). Following 10–20 min of illumination, the dish is imaged again using the same filters used in the first step. The digital images are loaded into Image Pro plus software (Media Cybernetics, Bethesda, MD), where they are aligned and processed using a custom macro. The output of the macro is a list of the mean intensities for each colony in each of the four images. These data are imported into Microsoft Excel, where they are plotted as green fluorescence before photoconversion *versus* red fluorescence after photoconversion. Colonies that exhibited the highest intensities in both channels were picked and used as templates for the following round of library creation.

Protein purification and characterization

Protein purification was carried out as previously described,[24] and the buffer was changed into phosphate-buffered saline (PBS; pH 7.4). Samples of mClavGR2, Dendra2, and mEos2 used for determination of oligomeric structure were first subjected to an additional step of purification on a HiLoad 16/60 Superdex 75 pg column (GE Healthcare). Molar extinction coefficients (ε) of the green states were measured by alkali denaturation method and then used as reference to measure ε for the red states.[35,40] Fluorescence quantum yields (Φ) were determined using fluorescein in 10 mM NaOH ($\Phi = 0.95$)[41] and Rhodamine 6G in ethanol ($\Phi = 0.94$)[42] as standards. For determination of pH dependence, purified protein in PBS was diluted 1:50 into a series of pH-adjusted citrate saline (pH ≤ 8) or sodium phosphate (pH >8) buffers in a 96-well black clear-bottom plate (Corning). Fluorescence was measured using a Safire2 plate reader (Tecan).

The oligomeric structures of mClavGR variants, mEos2, and Dendra2 were determined by gel-filtration chromatography with a HiLoad 16/60 Superdex 75 pg gel-filtration column on an AKTAbasic liquid chromatography system (GE Healthcare). Samples of dimeric dTomato and monomeric mCherry proteins[35] were expressed and purified in the same way as mClavGR variants and used as size standards. Purified mClavGR variants were mixed with dTomato or mCherry, and the resulting elution profiles were monitored at 488 nm for mClavGR variants, at 555 nm for dTomato, and at 585 nm for mCherry.

To measure the maturation profiles of mClavGR1, mClavGR2, mEos2, and Dendra2 (Clontech), we cultured *E. coli* transformed with pBAD/His B plasmids bearing the encoding cDNA overnight in glucose-supplemented LB media to prevent gene expression. The culture was diluted to an OD_{600} of 0.6, purged with argon for 20 min, sealed with a rubber septum, and incubated for another 1 h to allow thorough consumption of the residue oxygen. Arabinose (0.25%) was then added via a syringe with needle to induce expression of the FPs. After 4.5 h of incubation with shaking at 37 °C, the cultures were transfered to an ice bath for 10 min and maintained at 4 °C, unless indicated otherwise. Cells were centrifuged at 8000 rpm for 2 min, and cell pellets were lysed using vacuum-degassed B-PER II (Pierce) and incubated at room temperature for 12 min. The lysate was then centrifuged at 12,500 rpm for 5 min, and the supernatant was diluted five times into PBS (pH 7.4). Fluorescence maturation was monitored at 37 °C using a Safire2 plate reader (Tecan).

To determine the relative quantum yields for photoconversion, we measured each purified variant's absorbance at 487 nm to determine the concentration. The proteins were then converted into the red state by the same illumination system used for screening for 1 min. The absorbance at 565 nm of the photoconverted proteins was measured to determine the concentration of the photoconverted red species. The proteins were then diluted 10-fold into PBS, and their red fluorescence was recorded. The photoconversion quantum yield relative

to mClavGR1 ($\Phi_{PC,GRX}/\Phi_{PC,GR1}$) was calculated using Eq. (1):

$$\frac{\Phi_{PC,GRX}}{\Phi_{PC,GR1}} = \frac{C_{red,GRX} / C_{green,GRX}}{C_{red,GR1} / C_{green,GR1}} = \frac{A_{565,GRX} / \varepsilon_{565,GRX}}{A_{487,GRX} / \varepsilon_{487,GRX}} \frac{A_{487,GR1} / \varepsilon_{487,GR1}}{A_{565,GR1} / \varepsilon_{565,GR1}} \quad (1)$$

In Eq. (1), A_{487}, A_{565}, ε_{487}, and ε_{565} are the absorbance and extinction coefficients at 487 nm (before photoconversion) and 565 nm (after photoconversion), respectively. GR1 refers to mClavGR1, while GRX refers to one of the other variants. This relative photoconversion quantum yield gives the frequency of generation of the red species of the evolved variants relative to the parent mClavGR1 when illuminated by the screening system. Relative photoconversion effectiveness ($E_{PC,GRX}/E_{PC,GR1}$) was calculated using Eq. (2), again with mClavGR1 as reference:

$$\frac{E_{PC,GRX}}{E_{PC,GR1}} = \frac{c_{GR1} I_{GRX}}{c_{GRX} I_{GR1}} \quad (2)$$

In Eq. (2), c is the concentration of the purified protein solution, and I is the red fluorescence intensity following photoconversion. This relative photoconversion efficiency can differ from the photoconversion yield due to additional factors such as the ratio of neutral form to anionic form at the beginning and the brightness of the red state. All absorption measurements were acquired on a DU-800 UV–visible spectrophotometer (Beckman). All fluorescence spectra were recorded on a QuantaMaster spectrofluorimeter (Photon Technology International) and corrected for detector response.

Laser scanning confocal microscopy photobleaching experiments were conducted with N-terminal fusions of the appropriate FP to human H2B (six-residue linker) to confine fluorescence to the nucleus. HeLa-S3 cells (average nucleus diameter, 17 μm) were transfected with the H2B construct using Effectene (Qiagen) and maintained in a 5% CO_2 atmosphere in Bioptechs Delta-T imaging chambers for at least 36 h prior to imaging. The chambers were transferred to a Bioptechs stage adapter, imaged at low magnification to ensure cell viability, and then photobleached using a 40× oil immersion objective (numerical aperture, 1.00; Olympus UPlan Apo). Laser lines (543 nm, He–Ne; 488 nm, argon ion) were adjusted to an output power of 100 μW and measured with a FieldMax II-TO (Coherent) power meter equipped with a high-sensitivity silicon/germanium optical sensor (Coherent OP-2Vis). The instrument (Olympus FV1000) was set to a zoom of 4×, a region of interest of 341.2 μm^2 (108×108 pixels), a photomultiplier voltage of 700 V, and an offset of 5%, with a scan time of 0.181 s per frame. Nuclei having approximately the same dimensions and intensity under the fixed instrument settings were chosen for photobleaching assays. Using the 543-nm laser (mClavGR2 red species), we recorded fluorescence emission with a 570-nm dichromatic mirror and a 590-nm longpass barrier filter, whereas emission using the 488-nm laser (mClavGR2 green species) was directly reflected by a mirror through a 510-nm longpass barrier filter.

For wide-field fluorescence photobleaching, Bioptechs imaging chambers containing HeLa cells expressing mClavGR2 fusion to H2B were transferred to a stage adapter (Bioptechs) on a Nikon TE2000 wide-field inverted microscope equipped with an Exacte metal halide lamphouse (EXFO, Mississauga, Ontario, Canada) and imaged at low magnification (20×) to ensure cell viability. Selected regions containing 5–20 nuclei were photobleached using the neutral density settings on the metal halide lamphouse and a 40× Plan Fluor objective (numerical aperture, 0.75), recording images at 1-s intervals using a QImaging Retiga EXi camera system (Photometrics, Tucson, AZ). Photobleaching was conducted before and after photoconversion of mClavGR2 using Omega QMax Blue filter sets. For wide-field photobleaching of the green state, a Chroma FITC-HYQ cube was used with measured power at an objective of 202.6 mW/cm^2. For wide-field photobleaching of the red state, a Semrock TRITC-A-000 cube was used with measured power at an objective of 489.9 mW/cm^2. Light power at the objective output was measured with a Newport (Irvine, CA) 1918-C optical power meter coupled to a silicon photodetector (918-D-SL-OD3). The illumination power was adjusted using Exacte neutral density filters to ensure that the same power levels were used for each filter set. Wide-field photobleaching raw data were collected with NIS-Elements software (Nikon) and analyzed with Simple PCI software (Hamamatsu), as previously described.[43]

Mammalian expression vectors

To create the mClavGR2-actin and mClavGR2-NLS vectors, we amplified the gene-encoding mClavGR2 with a 5′ primer with an NheI site and a 3′ primer with an XhoI site. The purified PCR products were then digested and ligated into pEGFP-actin and pEYFP-NLS (Clontech), whose FP-coding gene has been previously removed by the same restriction enzymes. To create the mClavGR2 vector for cytoplasmic expression, we inserted the mClavGR2 gene between the XhoI restriction site and the EcoRI restriction site of a modified pcDNA3 vector (Invitrogen) in which the multiple cloning site had been modified to contain XhoI and EcoRI restriction sites in the same reading frame as the identical sites in pBAD/His B. The full-length ICAM-1 (Addgene plasmid 8632)[44] and mClavGR2 cDNA were incorporated into the modified pcDNA3 vector mentioned above, with a 24-amino-acid linker between them. The linker's sequence is KALSAAAGGGGSGGGGSGGGGSEF.[45]

All other mClavGR2 fusion expression vectors were constructed using C1 and N1 (Clontech style) cloning vectors, as previously described.[34] The mClavGR2 cDNA was amplified with a 5′ primer encoding an AgeI site and a 3′ primer encoding either a BspEI (C1) site or an NotI (N1) site. The purified and digested PCR products were ligated into similarly digested EGFP-C1 and EGFP-N1 cloning vector backbones. To generate fusion vectors, we digested the appropriate mClavGR2 cloning vector and an EGFP fusion vector, either sequentially or doubly, with the appropriate enzymes and ligated them together after gel purification. Thus, to prepare mClavGR2 N-terminal fusions, we performed the following digests: human nonmuscle α-actinin, EcoRI and NotI (fusion cDNA source; Tom Keller, The Florida State University); rat α-1 Cx43, EcoRI and BamHI (Matthias Falk, Lehigh University); human H2B, BamHI and NotI (George Patterson, National Institutes of Health); N-terminal 81 amino acids of human β-1,4-galactosyltransferase, BamHI and NotI (Golgi; Clontech); human keratin 18, EcoRI and NotI (Open Biosystems, Huntsville, AL); human zyxin, BamHI and NotI (Clare Waterman, National Institutes of Health); lifeact, BamHI and NotI (Integrated DNA Technologies); human VE cadherin (Origene, Rockville, MD); chicken c-src (Marilyn Resh, Sloan-Kettering, New York). To prepare mClavGR2 C-terminal fusions, we performed the following digests: human β-actin, NheI and BglII (Clontech); human lamin B1, NheI and BglII (George Patterson, National Institutes of Health); human fibrillarin, AgeI and BglII (Evrogen); mouse

CAF1, NheI and BglII (Akash Gunjan, The Florida State University); mouse microtubule binding domain of MAP4, NheI and BglII (Richard Cyr, Penn State University); endoplasmic reticulum, AgeI and BspEI (Integrated DNA Technologies); c-Ha-Ras (CAAX), AgeI and BspEI (membrane; Clontech). DNA for mammalian transfection was prepared using the Plasmid Maxi kit (Qiagen). Morphological features in all fusion constructs were confirmed by imaging fixed cell preparations on coverslips using a Nikon 80i upright microscope with ET-GFP and/or ET-DsRed filter sets (Chroma) coupled to a Hamamatsu Orca ER camera.

Cells and transfection

HeLa cells were maintained in Dulbecco's modified Eagle's medium (DMEM; Invitrogen) supplemented with 10% heat-inactivated fetal calf serum (FCS; Invitrogen) and 2 mM GlutaMax (Invitrogen) at 37 °C and 5% CO_2. Jurkat cells (clone E6.1) were maintained in RPMI 1640 (Invitrogen) supplemented with 10% FCS. Plasmid DNA for transfection was prepared by Qiagen Plasmid Midi Kit (Qiagen) in accordance with the manufacturer's protocol. Lipofectamine 2000 (Invitrogen) was used as transfection reagent. Cells for transfection and imaging were cultured on 35-mm glass-bottom culture dishes. The transfection protocol was essentially performed as recommended by the manufacturer, but used 3 μg of plasmid DNA, 7.5 μl of transfection reagent, and 2.5 h of incubation time (incubation of the cell with the transfection reagent). The medium was changed into Hepes-buffered Hank's buffered salt solution (Invitrogen) before imaging. Imaging was performed 24–36 h after transfection. To examine the localization of fusions and dynamics in live cell imaging and photobleaching measurements, we grew HeLa or LLC-PK1 (pig kidney epithelial; ATCC, Manassas, VA) cells in a mixture of DMEM and Ham's F-12 (50:50) containing 12% Cosmic calf serum (Hyclone) to 70% confluence and transfected them with 1 μg of the appropriate vector DNA using Effectene (Qiagen) in accordance with the manufacturer's instructions. The medium was changed after 24 h, and cells exhibiting normal morphology were imaged after 36 h.

Live cell imaging

Fluorescence microscopy of mClavGR2 diffusion in the cytoplasm was performed using an inverted Nikon Eclipse Ti microscope equipped with an QuantEM 512SC electron-multiplying CCD (Photometrics), a 75-W xenon lamp for epifluorescence illumination, a 63× oil immersion objective (Nikon), and a 408-nm photoactivation laser with a power of >500 mW (Melles Griot).

Laser scanning confocal imaging of mClavGR2 dynamics was conducted on an Olympus FV1000 microscope equipped with a photoactivation (SIM) scanner emitting at 405 nm. Fusions were imaged with a 488-nm argon ion laser (Melles Griot) before photoconversion and with a helium–neon 543-nm laser (Melles Griot) after photoconversion, using detector slit settings of 510–540 nm and 590–650 nm, respectively. Videos were processed using Adobe Premier and After Effects.

Imaging of ICAM-1-mClavGR2 diffusion

Jurkat cells were pretreated with phorbol 12-myristate 13-acetate at a concentration of 50 ng/ml for 30 min at 37 °C. The stimulated Jurkat cells were centrifuged and resuspended in DMEM/10% FCS/GlutaMax. Approximately 10^6 Jurkat cells were added to a 35-mm glass-bottom culture dish containing HeLa cells previously transfected with the ICAM-1-mClavGR2 plasmid. The cell mixture was incubated at 37 °C for another 30 min to allow adhesion, and the solution was exchanged to remove Jurkat cells remaining in suspension. Imaging was performed on a Perkin-Elmer Ultraview ERS system (Perkin-Elmer Life Sciences, Inc., Boston, MA) equipped with a Yokogawa (Yokogawa Corp., Japan) Nipkow spinning disk confocal system, a 60× oil immersion objective (Carl Zeiss), an electron-multiplying CCD (Hamamatsu), and a 20-mW 405-nm laser (Melles Griot). Temperature was maintained at 37 °C during acquisition. An exposure of approximately 40 ms at 15% laser power (405 nm) was used to photoconvert mClavGR2 within the defined area of interest. Four images of each of the green and red channels were acquired before photoconversion, followed by 10 s of acquisition at maximum speed, followed by 2 min at 3 s per frame for 2 min. The average intensity of the four images acquired before photoconversion was subtracted from the background-corrected red fluorescence intensity, which was then normalized to the first image after photoconversion. Fluorescence as a function of time ($F(t)$) was fitted with the equation:

$$F(t) = A + B\exp(-t/\tau) \quad (3)$$

where A and B correspond to the fractional contributions of immobile and mobile proteins, respectively, and τ is the time constant for the decay of fluorescence intensity. The diffusion half time ($t_{1/2}$) is 0.69τ.

Acknowledgements

This work was supported by Natural Sciences and Engineering Research Council of Canada Discovery grants (R.E.C. and C.W.C.) and a PetroCanada Young Innovator award to R.E.C. R.E.C. holds a Tier II Canada Research Chair in Bioanalytical Chemistry. The authors thank Ray Lemieux, Eric Flaim, Xuejun Sun, and Andreas Ibraheem at the University of Alberta for technical assistance, and Korey Wilson, Ericka Ramko, and Christopher Murphy at Florida State University for help with vector construction and imaging. The ICAM-1-encoding plasmid was provided by T. A. Springer (Department of Pathology, Harvard Medical School, Boston, MA). The mEos2 cDNA was provided by L. L. Looger (Janelia Farm Research Campus, Ashburn, VA).

Competing Financial Interests Statement. New FPs that originate from the Campbell lab and are described in this manuscript are covered by a US patent application owned by the University of Alberta. Allele Biotechnology is the Licensed distributor of plasmids containing genes encoding these FPs.

Supplementary Data

Supplementary data associated with this article can be found, in the online version, at doi:10.1016/j.jmb.2010.06.056

References

1. Ando, R., Hama, H., Yamamoto-Hino, M., Mizuno, H. & Miyawaki, A. (2002). An optical marker based on the UV-induced green-to-red photoconversion of a fluorescent protein. *Proc. Natl Acad. Sci. USA*, **99**, 12651–12656.
2. Wiedenmann, J., Ivanchenko, S., Oswald, F., Schmitt, F., Rocker, C., Salih, A. *et al.* (2004). EosFP, a fluorescent marker protein with UV-inducible green-to-red fluorescence conversion. *Proc. Natl Acad. Sci. USA*, **101**, 15905–15910.
3. Gurskaya, N. G., Verkhusha, V. V., Shcheglov, A. S., Staroverov, D. B., Chepurnykh, T. V., Fradkov, A. F. *et al.* (2006). Engineering of a monomeric green-to-red photoactivatable fluorescent protein induced by blue light. *Nat. Biotechnol.* **24**, 461–465.
4. Tsutsui, H., Karasawa, S., Shimizu, H., Nukina, N. & Miyawaki, A. (2005). Semi-rational engineering of a coral fluorescent protein into an efficient highlighter. *EMBO Rep.* **6**, 233–238.
5. Mizuno, H., Mal, T. K., Tong, K. I., Ando, R., Furuta, T., Ikura, M. & Miyawaki, A. (2003). Photo-induced peptide cleavage in the green-to-red conversion of a fluorescent protein. *Mol. Cell*, **12**, 1051–1058.
6. Ormo, M., Cubitt, A. B., Kallio, K., Gross, L. A., Tsien, R. Y. & Remington, S. J. (1996). Crystal structure of the *Aequorea victoria* green fluorescent protein. *Science*, **273**, 1392–1395.
7. Chattoraj, M., King, B. A., Bublitz, G. U. & Boxer, S. G. (1996). Ultra-fast excited state dynamics in green fluorescent protein: multiple states and proton transfer. *Proc. Natl Acad. Sci. USA*, **93**, 8362–8367.
8. Tsutsui, H., Shimizu, H., Mizuno, H., Nukina, N., Furuta, T. & Miyawaki, A. (2009). The E1 mechanism in photo-induced beta-elimination reactions for green-to-red conversion of fluorescent proteins. *Chem. Biol.* **16**, 1140–1147.
9. Chudakov, D. M., Verkhusha, V. V., Staroverov, D. B., Souslova, E. A., Lukyanov, S. & Lukyanov, K. A. (2004). Photoswitchable cyan fluorescent protein for protein tracking. *Nat. Biotechnol.* **22**, 1435–1439.
10. Kremers, G. J., Hazelwood, K. L., Murphy, C. S., Davidson, M. W. & Piston, D. W. (2009). Photoconversion in orange and red fluorescent proteins. *Nat. Methods*, **6**, 355–358.
11. Shaner, N. C., Patterson, G. H. & Davidson, M. W. (2007). Advances in fluorescent protein technology. *J. Cell Sci.* **120**, 4247–4260.
12. Lippincott-Schwartz, J., Altan-Bonnet, N. & Patterson, G. H. (2003). Photobleaching and photoactivation: following protein dynamics in living cells. *Nat. Cell Biol. Suppl.* S7–S14.
13. Lukyanov, K. A., Chudakov, D. M., Lukyanov, S. & Verkhusha, V. V. (2005). Innovation: photoactivatable fluorescent proteins. *Nat. Rev. Mol. Cell Biol.* **6**, 885–891.
14. Patterson, G. H. & Lippincott-Schwartz, J. (2002). A photoactivatable GFP for selective photolabeling of proteins and cells. *Science*, **297**, 1873–1877.
15. Ando, R., Mizuno, H. & Miyawaki, A. (2004). Regulated fast nucleocytoplasmic shuttling observed by reversible protein highlighting. *Science*, **306**, 1370–1373.
16. Patterson, G., Davidson, M., Manley, S. & Lippincott-Schwartz, J. (2010). Superresolution imaging using single-molecule localization. *Annu. Rev. Phys. Chem.* **61**, 345–367.
17. McKinney, S. A., Murphy, C. S., Hazelwood, K. L., Davidson, M. W. & Looger, L. L. (2009). A bright and photostable photoconvertible fluorescent protein. *Nat. Methods*, **6**, 131–133.
18. Hayashi, I., Mizuno, H., Tong, K. I., Furuta, T., Tanaka, F., Yoshimura, M. *et al.* (2007). Crystallographic evidence for water-assisted photo-induced peptide cleavage in the stony coral fluorescent protein Kaede. *J. Mol. Biol.* **372**, 918–926.
19. Campbell, R. E., Tour, O., Palmer, A. E., Steinbach, P. A., Baird, G. S., Zacharias, D. A. & Tsien, R. Y. (2002). A monomeric red fluorescent protein. *Proc. Natl Acad. Sci. USA*, **99**, 7877–7882.
20. Habuchi, S., Tsutsui, H., Kochaniak, A. B., Miyawaki, A. & van Oijen, A. M. (2008). mKikGR, a monomeric photoswitchable fluorescent protein. *PLoS One*, **3**, e3944.
21. Adam, V., Nienhaus, K., Bourgeois, D. & Nienhaus, G. U. (2009). Structural basis of enhanced photoconversion yield in green fluorescent protein-like protein Dendra2. *Biochemistry*, **48**, 4905–4915.
22. Nienhaus, K., Nienhaus, G. U., Wiedenmann, J. & Nar, H. (2005). Structural basis for photo-induced protein cleavage and green-to-red conversion of fluorescent protein EosFP. *Proc. Natl Acad. Sci. USA*, **102**, 9156–9159.
23. Nienhaus, G. U., Nienhaus, K., Holzle, A., Ivanchenko, S., Renzi, F., Oswald, F. *et al.* (2006). Photoconvertible fluorescent protein EosFP: biophysical properties and cell biology applications. *Photochem. Photobiol.* **82**, 351–358.
24. Ai, H., Henderson, J. N., Remington, S. J. & Campbell, R. E. (2006). Directed evolution of a monomeric, bright and photostable version of *Clavularia* cyan fluorescent protein: structural characterization and applications in fluorescence imaging. *Biochem. J.* **400**, 531–540.
25. Dai, M., Fisher, H. E., Temirov, J., Kiss, C., Phipps, M. E., Pavlik, P. *et al.* (2007). The creation of a novel fluorescent protein by guided consensus engineering. *Protein Eng. Des. Sel.* **20**, 69–79.
26. Fromant, M., Blanquet, S. & Plateau, P. (1995). Direct random mutagenesis of gene-sized DNA fragments using polymerase chain reaction. *Anal. Biochem.* **224**, 347–353.
27. Zhao, H. & Zha, W. (2006). *In vitro* 'sexual' evolution through the PCR-based staggered extension process (StEP). *Nat. Protoc.* **1**, 1865–1871.
28. Henderson, J. N. & Remington, S. J. (2005). Crystal structures and mutational analysis of amFP486, a cyan fluorescent protein from *Anemonia majano*. *Proc. Natl Acad. Sci. USA*, **102**, 12712–12717.
29. Shaner, N. C., Steinbach, P. A. & Tsien, R. Y. (2005). A guide to choosing fluorescent proteins. *Nat. Methods*, **2**, 905–909.
30. Chudakov, D. M., Lukyanov, S. & Lukyanov, K. A. (2007). Tracking intracellular protein movements using photoswitchable fluorescent proteins PS-CFP2 and Dendra2. *Nat. Protoc.* **2**, 2024–2032.
31. Dittrich, P. S., Schäfer, S. P. & Schwille, P. (2005). Characterization of the photoconversion on reaction of the fluorescent protein Kaede on the single-molecule level. *Biophys. J.* **89**, 3446–3455.
32. Adam, V., Lelimousin, M., Boehme, S., Desfonds, G., Nienhaus, K., Field, M. J. *et al.* (2008). Structural characterization of IrisFP, an optical highlighter undergoing multiple photo-induced transformations. *Proc. Natl Acad. Sci. USA*, **105**, 18343–18348.
33. Jung, G., Mais, S., Zumbusch, A. & Brauchle, C. (2000). The role of dark states in the photodynamics of the

green fluorescent protein examined with two-color fluorescence excitation spectroscopy. *J. Phys. Chem. A*, **104**, 873–877.
34. Ai, H., Olenych, S. G., Wong, P., Davidson, M. W. & Campbell, R. E. (2008). Hue-shifted monomeric variants of *Clavularia* cyan fluorescent protein: identification of the molecular determinants of color and applications in fluorescence imaging. *BMC Biol.* **6**, 13.
35. Shaner, N. C., Campbell, R. E., Steinbach, P. A., Giepmans, B. N., Palmer, A. E. & Tsien, R. Y. (2004). Improved monomeric red, orange and yellow fluorescent proteins derived from *Discosoma* sp. red fluorescent protein. *Nat. Biotechnol.* **22**, 1567–1572.
36. Yang, L., Kowalski, J. R., Yacono, P., Bajmoczi, M., Shaw, S. K., Froio, R. M. *et al.* (2006). Endothelial cell cortactin coordinates intercellular adhesion molecule-1 clustering and actin cytoskeleton remodeling during polymorphonuclear leukocyte adhesion and transmigration. *J. Immunol.* **177**, 6440–6449.
37. Kanters, E., van Rijssel, J., Hensbergen, P. J., Hondius, D., Mul, F. P., Deelder, A. M. *et al.* (2008). Filamin B mediates ICAM-1-driven leukocyte transendothelial migration. *J. Biol. Chem.* **283**, 31830–31839.
38. Barreiro, O., Zamai, M., Yáñez-Mó, M., Tejera, E., López-Romero, P., Monk, P. N. *et al.* (2008). Endothelial adhesion receptors are recruited to adherent leukocytes by inclusion in preformed tetraspanin nanoplatforms. *J. Cell Biol.* **183**, 527–542.
39. Bang, D. & Church, G. M. (2008). Gene synthesis by circular assembly amplification. *Nat. Methods*, **5**, 37–39.
40. Ward, W. W. (1998). Biochemical and physical properties of GFP. In *Green Flourescent Protein: Properties, Application, and Protocols* (Chalfie, M. & Kain, S., eds), pp. 45–75, Wiley, New York, NY.
41. Brannon, J. H. & Magde, D. (1978). Absolute quantum yield determination by thermal blooming fluorescein. *J. Phys. Chem.* **82**, 705–709.
42. Fischer, M. & Georges, J. (1996). Fluorescence quantum yield of Rhodamine 6G in ethanol as a function of concentration using thermal lens spectrometry. *Chem. Phys. Lett.* **260**, 115–118.
43. Shaner, N. C., Lin, M. Z., McKeown, M. R., Steinbach, P. A., Hazelwood, K. L., Davidson, M. W. & Tsien, R. Y. (2008). Improving the photostability of bright monomeric orange and red fluorescent proteins. *Nat. Methods*, **5**, 545–551.
44. Staunton, D. E., Marlin, S. D., Stratowa, C., Dustin, M. L. & Springer, T. A. (1988). Primary structure of ICAM-1 demonstrates interaction between members of the immunoglobulin and integrin supergene families. *Cell*, **52**, 925–933.
45. Wülfing, C., Sjaastad, M. D. & Davis, M. M. (1998). Visualizing the dynamics of T cell activation: intracellular adhesion molecule 1 migrates rapidly to the T cell/B cell interface and acts to sustain calcium levels. *Proc. Natl Acad. Sci. USA*, **95**, 6302–6307.